

Transport through double-gated graphene-based devices

S Russo^{1,2}, M F Craciun¹, M Yamamoto¹, S Tarucha^{1,3} and A F Morpurgo⁴

¹ Department of Applied Physics, The University of Tokyo, Tokyo 113-8656, Japan

² Kavli Institute of Nanoscience, Delft University of Technology, Lorentzweg 1, 2628 C J Delft, The Netherlands

³ Quantum Spin Information Project, ICORP, Japan Science and Technology Agency, Atsugi-shi, 243-0198, Japan

⁴ DPMC and GAP, University of Geneva, quai Eriste-Ansermet 24, CH-1211 Geneva 4, Switzerland

E-mail: s.russo@tnw.tudelft.nl

Abstract.

We discuss transport through double gated single and few layer graphene devices. This kind of device configuration has been used to investigate the modulation of the energy band structure through the application of an external perpendicular electric field, a unique property of few layer graphene systems. Here we discuss technological details that are important for the fabrication of top gated structures, based on electron-gun evaporation of SiO_2 . We perform a statistical study that demonstrates how { contrary to expectations} the breakdown field of electron-gun evaporated thin SiO_2 films is comparable to that of thermally grown oxide layers. We find that a high breakdown field can be achieved in evaporated SiO_2 only if the oxide deposition is directly followed by the metallization of the top electrodes, without exposure to air of the SiO_2 layer.

1. Introduction

The ability to isolate and embed single- and multi-layer graphene in double gated structures is paving the way to reveal unique electronic properties of these systems [1, 2, 3, 4, 5, 6, 7, 8, 9, 10, 11, 12, 13]. The ability to change the voltages applied to a nano-fabricated top gate and to the back-gate offers the possibility to gain local control of the charge density and of imposing locally a perpendicular electric field. This device configuration was used recently to show how the band structure of graphene-based materials can be tuned continuously [8, 12]. In particular, bilayer graphene exhibits an electric field induced insulating state due to the opening of a gap between valence and conduction band [8], and in trilayers the band-overlap can be increased substantially [12]. Cleverly designed top gates on a graphene single layer have also been used successfully for engineering p-n junctions [1, 2, 3, 5, 6, 7], necessary for the investigation of Klein tunneling [1, 3, 4], and to attempt the fabrication of controlled quantum dots [15, 16]. Key to the fabrication of top gated structures is the ability to deposit good quality thin gate oxides, with high breakdown field and low leakage current.

Here, after reviewing the relevance of double gated devices on the electric field modulation of the band structure of double and triple layer graphene, we discuss in some details technological aspects related to the properties of the SiO_2 layers used as gate insulators. In particular, we discuss how we can routinely achieve high breakdown fields in electron-gun evaporated thin SiO_2 films (15 nm), comparable to the breakdown fields of thermally grown SiO_2 , which is surprising giving that SiO_2 deposited by evaporation was long believed to be a poor quality insulator. To unveil the reasons behind the good insulating quality of our evaporated SiO_2 films, we conducted a statistical study of leakage current and breakdown voltage in capacitors, where two metallic electrodes are separated by a SiO_2 layer fabricated in different ways. We demonstrate that if SiO_2 and top gate metal electrodes are deposited subsequently without exposing the SiO_2 to air, the electrical performance of electron-gun evaporated SiO_2 is comparable to that of thermally grown SiO_2 . In contrast, exposure to air of the SiO_2 layer before deposition of the counter-electrode leads to much worse insulating characteristics. Our findings indicate that extrinsic degradation (probably due to the absorption of humidity) has limited in the past the insulating quality of electron-gun evaporated SiO_2 .

2. Device and fabrication

Single and few layer graphene flakes used for the device fabrication were obtained by micro-mechanical cleavage of natural graphite crystals, and by their subsequent transfer onto a highly doped Silicon substrate (acting as a gate) covered by a 285 nm thick thermally grown SiO_2 layer. The thickness of the graphene layers can be simply identified by analyzing the shift in intensity in the RGB green channel relative to the substrate (i.e. Relative Green Shift) [8, 12, 14, 17, 18]. A plot of the relative green shift, as extracted from optical microscope images of various samples taken with a digital

camera, exhibits plateaus corresponding to the discrete thickness values –see Fig. 1a. Subsequent transport measurements (quantum Hall effect, resistance dependence on a perpendicular electric field, etc.) confirm the validity of this optical method (Fig. 1b). The fabrication of nanostructures is accomplished by conventional electron-beam lithography. Metallic contacts and top gates were deposited by electron-gun evaporation, respectively of Ti/Au (10=25nm thick with a back ground pressure of 9×10^7 torr) for contacts and SiO₂/Ti/Au (15=10=25nm thick with a back ground pressure of 3×10^7 torr) for top gates, followed by lift-off. We took special care to fabricate all the ohmic contacts within 60 nm from the edges of the top gated areas, so that two probe resistance measurements are dominated by the resistance of the double gated region [19]. All transport measurements in double gated devices (see Fig. 1c) were made using a lock-in technique (excitation frequency: 19.3Hz), in the linear transport regime, at temperatures ranging from 300 mK up to 150K.

To understand why, contrary to expectations, we manage to achieve high breakdown field in thin, electron-beam evaporated SiO₂ films, we conducted a macroscopic breakdown study on two types of capacitor test structures. The first –which we refer to as type A– is characterized by subsequent evaporation of SiO₂/Ti/Au without breaking the vacuum in between the deposition of the different materials. For the second –type B SiO₂– we exposed the device to ambient for one hour after the SiO₂ deposition, before evaporating the Ti/Au counter electrode. The breakdown test measurements were made with a Keithley-2400 on more than 130 different capacitors (with three different surface areas: 125 × 115 m², 175 × 150 m² and 215 × 195 m²).

3. Transport experiments in double gated few layer graphene devices

The measurement configuration used for double gated devices is shown in Fig. 1c. A finite voltage applied to either one of the gates (back or top gate) changes the position of the Fermi level in the corresponding gated region of the graphene layer, by an amount corresponding to the induced charge density. In addition, by biasing the two gate electrodes with opposite polarity, a large external electric field applied perpendicular to the layer is generated, which is equal to $E_{ex} = (V_{bg} - V_{tg})/d_{tot}$ ($d_{tot} = 15 + 285$ nm is the total SiO₂ thickness). In this device configuration, we can monitor the evolution of the in plane transport properties for each few layer graphene device as a function of E_{ex} . Fig. 1d, e and f show the typical behavior of the square resistance measured respectively in double gated single (d), double (e) and triple (f) layer graphene, when sweeping one of the gates (back or top), while keeping the other gate at a fixed potential. It is apparent that the overall electric field dependence of R_{sq} is markedly distinct for graphene layers of different thickness. In all cases, the resistance exhibits a maximum (R_{sq}^{max}) whose value and position in gate voltage depend on the voltage applied to the gate on which a fixed potential is applied during the measurement. At $E_{ex} = 0$ V/m we find that for single and bilayer graphene $R_{sq}^{max} \approx 6$ K, close to a conductance per square of $4e^2/h$, as expected, indicating that the fabrication of top gate structures does not damage signif-

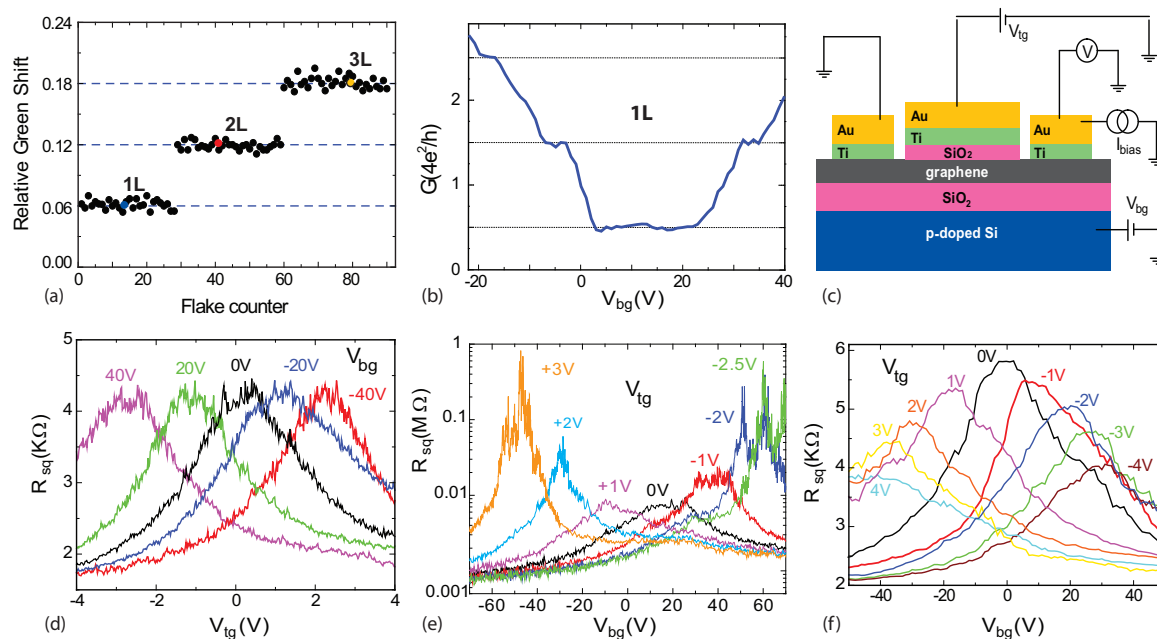


Figure 1. Panel (a) shows a plot of Relative Green Shift (as defined in the main text) for 90 few layer graphene areas, showing clear plateaus for graphene layer of different thickness. Panel (b) shows the conductance of a device (indicated by the blue dot in the plot shown in panel (a)) measured in the presence of high magnetic field; plateaus are observed at conductance values characteristic for Dirac electrons, indicating that flakes with Relative Green Shift = 0.06 are indeed single layers. Panel (c) shows a schematic representation of double-gated graphene devices, together with the measurement configuration used to study transport as a function of voltages applied to the top and back gates. Panels (d), (e) and (f) show plots of the square resistance in single (d), double (e) and triple (f) layers respectively, measured while sweeping one of the gates, for different fixed voltages applied on the other gate (for single layer $T = 300\text{mK}$, $W = 2\ \mu\text{m}$, $L = 1.4\ \mu\text{m}$, $\mu = 3500\text{cm}^2/\text{Vs}$, double layer $T = 300\text{mK}$, $W = 1.7\ \mu\text{m}$, $L = 1\ \mu\text{m}$, $\mu = 900\text{cm}^2/\text{Vs}$ and for triple layer $T = 1.5\text{K}$, $W = 1\ \mu\text{m}$, $L = 1.4\ \mu\text{m}$, $\mu = 800\text{cm}^2/\text{Vs}$).

icantly the material (for trilayers the square resistance is somewhat lower, owing to the presence of an overlap between valence and conduction band). Increasing the external electric field induces a well defined –and different– response for the square resistance layers of different thickness. Respectively, in a single layer R_{sq}^{max} is not affected by a finite E_{ex} ; in bilayers at low temperature R_{sq}^{max} increases from 6K to very large values ($> 1\ \text{M}\ \Omega$); in trilayers R_{sq}^{max} decreases with increasing E_{ex} . This experimental findings provides a clear indication that each few layer graphene is a unique material system, with distinct electronic properties.

Transport measurements over a wide range of temperatures (from 300mK up to 150K) underline the unique electronic properties of these few layer graphene devices. In bilayer graphene the larger E_{ex} , the larger is the temperature dependence of R_{sq}^{max} , see Fig. 2a and b. At $E_{ex} = 0\ \text{V/m}$, R_{sq}^{max} is only weakly temperature dependent (as it is typical of zero-gap semiconductors), and at $E_{ex} \neq 0\ \text{V/m}$ the observed behavior is the one typical

of an insulating state. On the contrary, trilayer graphene devices display a decrease of R_{sq}^{max} when lowering the temperature, stemming for the semimetallic nature of the constituent material.

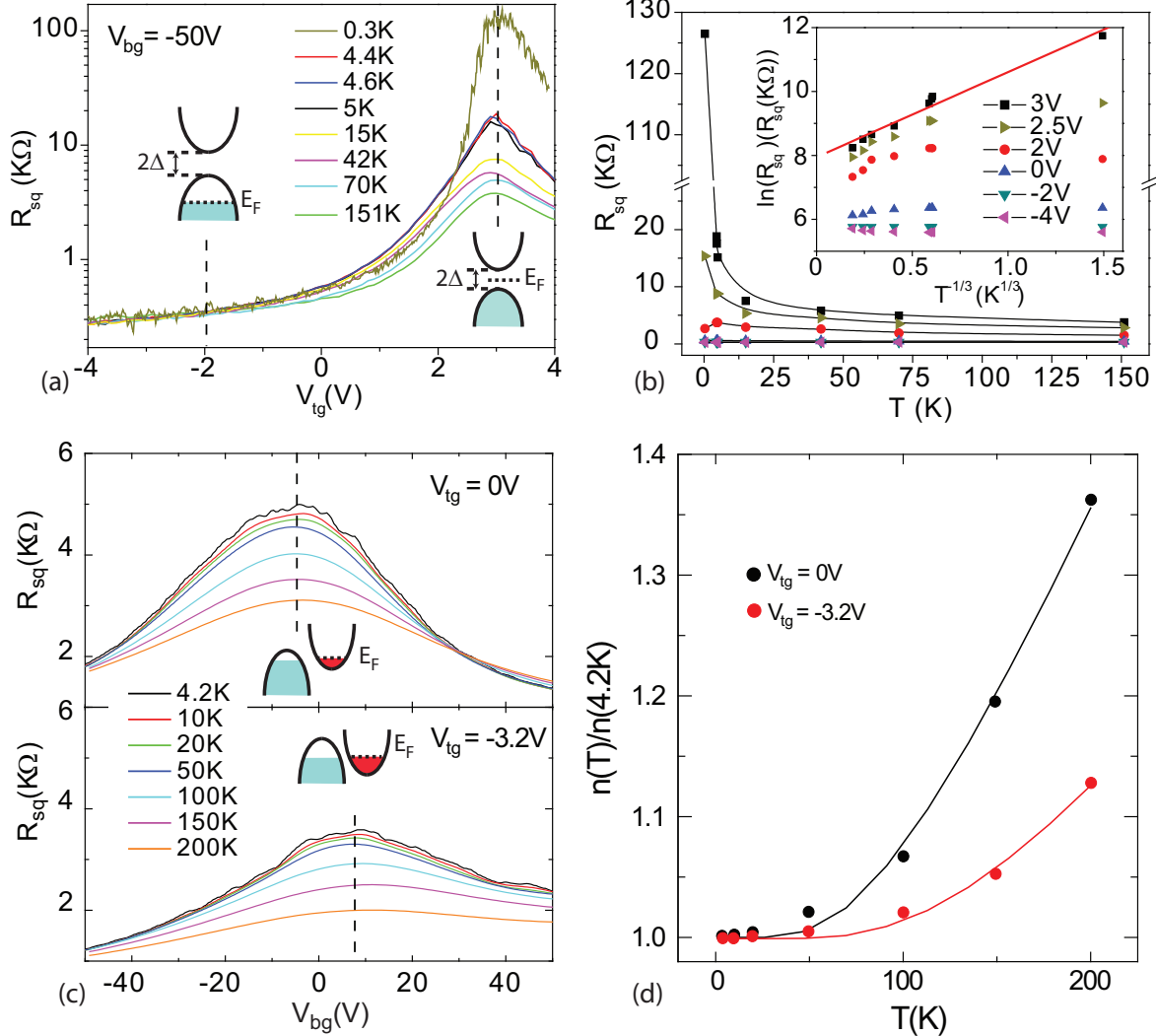


Figure 2. Panels (a) and (c) show plots of the square resistance at different temperatures for the bilayer and trilayer devices whose data are shown in panel (e) and (f) of Fig. 1. Panel (b) shows a plot of R_{sq} vs. T and $\ln(R_{sq})$ vs. $T^{1/3}$ extracted from the measurements shown in panel (a), at $V_{bg} = -50V$ and different V_{tg} values. Panel (d) shows the normalized charge density as a function of temperature, extracted from the trilayer measurements of panel (c). The continuous line is a fit based on a two-band model with finite overlap (see main text).

At a more quantitative level we find that R_{sq}^{max} in bilayer graphene is well described by $\propto \exp(T_0/T)^{1=3}$, with $T_0 \approx 20$ K at the maximum applied external electric field (see inset in Fig. 2b). This temperature dependence is indicative of variable-range hopping in a two dimensional material where an energy gap has opened, and where disorder

causes the presence of sub-gap states [8]. The opening of a gap in bilayer graphene at finite E_{ex} is also evident from the evolution of the temperature dependence of R_{sq} as a function of charge density, when the Fermi level is shifted from conduction to valence band, across the energy gap (see Fig 2b). The temperature dependence of the resistance in trilayer graphene is opposite to the one observed in bilayers, and it reveals that this material system is a semiconductor with a finite overlap (Δ) between conduction and valence band. This band overlap can be estimated within a two band model [12, 20, 21], where the number of thermally excited carriers increases with temperature according to $n(T) = (16 m^* \hbar^2 c) k_B T \ln(1 + e^{-\Delta/2k_B T})$ (m^* effective mass and c equal to twice the layer spacing). Measurements at finite E_{ex} show that Δ decreases when increasing external electric field (Δ goes from 32 meV to 52 meV in the measurements of Fig 2d). These experiments demonstrate that a perpendicular electric field applied on few layer graphene is a valuable tool to change the band structure of these materials. Double gated structures lead to the discovery of the only known electric field tunable insulator, i.e. bilayer graphene, and of the only known electric field tunable semiconductor, i.e. trilayer graphene.

4. Evaporated Silicon oxide as top gate dielectric

The opening of a sizeable band gap in bilayer graphene, and large changes in the band overlap of graphene trilayers require the application of large external electric fields to these material systems. It is the breakdown field of the gate-dielectric that imposes a limit to the maximum value of E_{ex} experimentally accessible in double gated structures. To optimize this aspect of the devices, we conducted a systematic study of the breakdown electric field of SiO_2 gate oxide for devices with different areas, fabricated under different conditions. Here we discuss the details of this investigation. From our statistical analysis we conclude that what is crucial is not the SiO_2 deposition method, but the details in the metallization of top gate electrodes afterwards, which affect the final quality of the oxide gate dielectric.

We compare devices fabricated following two different procedures. In devices of type A, the SiO_2 deposition and metallization processes were carried without breaking the vacuum, whereas in devices of type B, SiO_2 was exposed to air for one hour prior to the deposition of the Ti/Au gate electrode -i.e. the SiO_2/Ti . In all cases the devices were fabricated using a Si/ SiO_2 wafer coated with a Ti/Au film as substrate. Fig. 3a and b show various $I-V$ traces, measured in ambient condition, for type A and type B devices. A first clear difference between the two types of devices is the magnitude of the leakage current, visible by plotting the $I-V$ curves both in linear and logarithmic scale, see Fig. 3. For a surface area of $215 \times 195 \text{ nm}^2$, we find $I_{\text{leakage}} \approx 2.5 \times 10^{10} \text{ A} \cdot \text{m}^2$ for the best type B devices, one order of magnitude larger than that measured in the worse type A devices (the difference for typical devices are much larger than one order

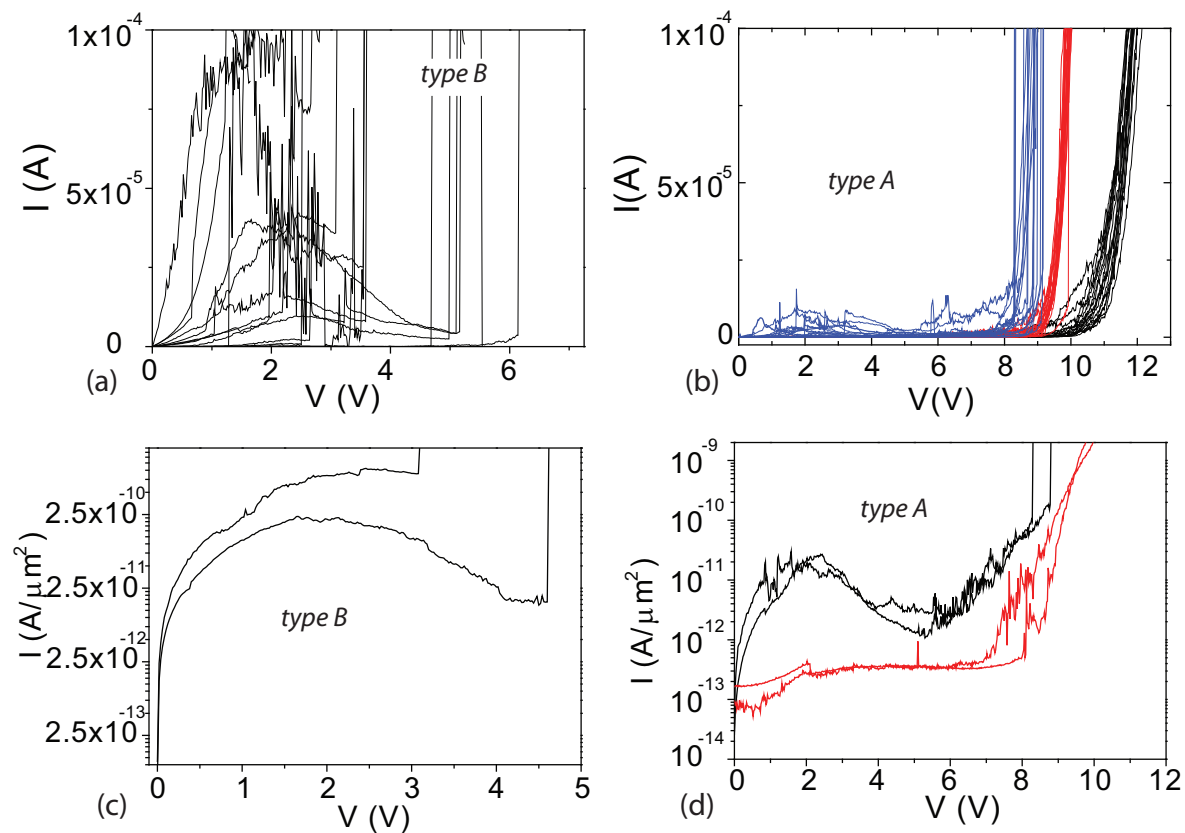


Figure 3. Panels (a) and (b) show I - V characteristics of respectively type B devices with $S = 215 \times 195 \text{ m}^2$ (a), and type A devices with $S = 215 \times 195 \text{ m}^2$ (blue curves), $S = 175 \times 150 \text{ m}^2$ (red curves) and $S = 125 \times 115 \text{ m}^2$ (black curves) (b). Panels (c) and (d) show the I - V curves in logarithmic scale for the two types of devices and areas $S = 215 \times 195 \text{ m}^2$ (black curves in (c) (d)) and $S = 175 \times 150 \text{ m}^2$ (red curves in (d)).

of magnitude). This extremely different level of leakage current already indicates that the exposure of SiO_2 to air previous to the deposition of top metals has a large negative influence on the insulating performance of the oxide.

The I - V characteristics further show that for a fixed surface area ($215 \times 195 \text{ m}^2$), the breakdown voltage V_{BD} for type A is typically in the range $8\text{V} < V_{BD} < 9\text{V}$ whereas type B devices breakdown anywhere in the range $0\text{V} < V_{BD} < 6\text{V}$. The differences in the failure of device types are best summarized in the histogram plots of V_{BD} - see Fig. 4a. For type B we find a large spreading in the distribution of V_{BD} , in contrast to the narrow distribution characteristic of type A devices. Furthermore, the comparison of V_{BD} for type A devices with different surface areas shows that V_{BD} increases slightly with decreasing the device area, possibly indicating that the properties of SiO_2 in type A close to breakdown are determined by small defects present in the film with rather small probability. However, we cannot rule out that the differences between the different sample populations originate from small differences (2-3 nm) in the thickness

of the SiO_2 layers. Note, in fact, that the leakage currents of these devices at low bias has only small sample-to-sample fluctuations, suggesting that the SiO_2 layers in type A devices are very uniform.

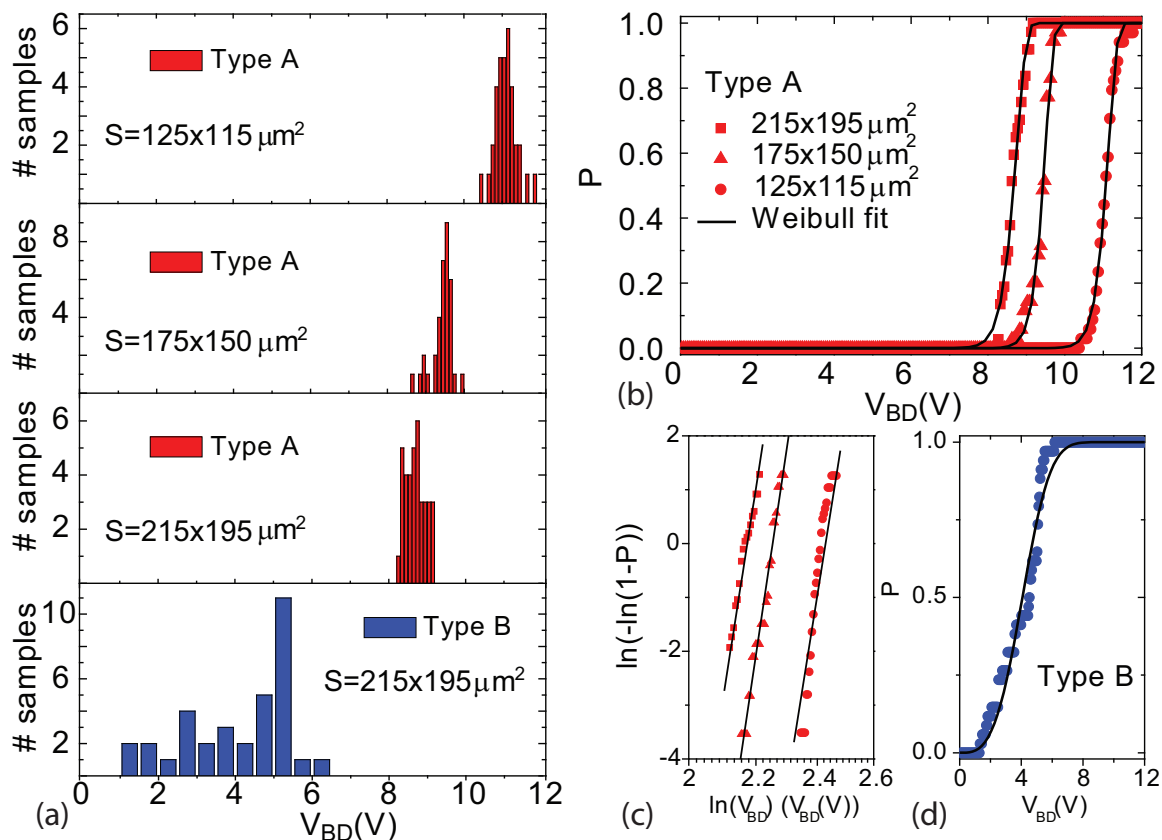


Figure 4. Panel (a) shows histogram plots of the breakdown field for different populations of test devices as specified in the legends. The panels in (b) and (c) show the cumulative probability for type A devices for different surface areas (dots are experimental data, and the continuous line is a fit to the Weibull distribution). The plot in (d) is a fit to the cumulative probability for type B devices ($S = 215 \times 195 \mu\text{m}^2$) to the Weibull distribution.

To try to quantify better our observations and analyze the role played by the specific fabrication technique and surface areas on the device performance (e.g. breakdown field), we adopt a failure analysis methodology [23]. In what follows we provide a statistical description of the breakdown probability introducing the cumulative probability (P) as the probability of a device to breakdown at a given voltage. From failure methodology, we notice that possibly the most suitable distribution for the failure of a population of samples, is the Weibull distribution [23, 24] $P = 1 - \exp[-(V_{BD} - V_0)^{\beta} (S/S_0)^{\alpha}]$ (S capacitor surface area, S_0 reference surface area, and V_0 are the Weibull parameters). The parameter β , also known as Weibull shape parameter, determines the shape of the probability density function -i.e. higher β indicates distributions with low dispersion of

$V_{BD} \cdot V_0$ is the Weibull scale parameter, whose only effect is to scale the V_{BD} distribution (the larger V_0 , the more "stretched" the distribution). Depending on the value of the Weibull parameters, this distribution mimics the behavior of other statistical distributions such as the normal and the exponential. Given a sample population, the Weibull parameters contain notion of the failure probability. Both β and V_0 are strongly affected by the failure mechanism which can eventually be identified when comparing the Weibull parameters for different sample populations. For instance, a value of β that does not depend on the capacitor surface area -i.e., the variance does not change with the surface area-, means that the microscopic mechanism of breakdown is common to all the samples, independent of the specific area [24].

The good agreement between a fit to the Weibull distribution of the cumulative probability for each different surface area and device types shows that the data of each different device population is well described by the Weibull distribution. To evaluate whether a single Weibull scaling law can explain breakdown results for all the different surfaces, we notice that -for type A- we can fit all the cumulative probability distributions with the same value $\beta = 52$, see Fig. 4b. This is made apparent by plotting $\ln(-\ln(1-P)) = \ln(S/S_0) = \ln(V_0) + \ln(V_{BD})$ as a function of $\ln(V_{BD})$ for data sets corresponding to different surface areas. Fig. 4b and c show clearly that all the data are lined up on parallel linear slopes (i.e., β is the same in all these cases). This finding implies that the breakdown mechanism is the same for all studied surface areas. Note that V_0 varies slightly with surface area, and that, as mentioned above, we cannot exclude that the origin of these variations is a small difference in the thickness of the SiO_2 layers for the different device populations (a difference of 2-3 nm would suffice to explain this observation).

We notice that $\beta = 52$ -estimated from the fit in Fig. 4b and c- is comparable to values found for thermally grown thin SiO_2 films, and it is compatible with failure of the devices due to surface roughness [22] probably being transferred to the dielectric film from the Ti/Au substrate. This quantitative analysis make it possible to state that electron-beam evaporated SiO_2 , directly coated by a metallic layer without exposure to air has an essentially identical quality to that of thermally grown oxide. A similar analysis of P for type B devices, gives a $\beta = 3.3$ -i.e. a much higher dispersion of breakdown field (see Fig. 4d). This small value for β in type B devices quantifies the much larger statistical spreading of the oxide properties in these devices. Since the only difference between type A and B devices is the fabrication step of the SiO_2/Ti interface, we conclude that exposure of the SiO_2 to air is indeed the cause for the poor insulating qualities. Indeed it is well known that SiO_2 is a hygroscopic material, that easily absorbs humidity in air. The humidity absorbed can affect the composition of the entire layer providing paths for the leakage current, and creating weak spots at which breakdown occurs already at low voltage.

5. Conclusions

In conclusion we have briefly reviewed transport in double gated bilayer and trilayer graphene devices. Motivated by the need for large electric fields, we have conducted a statistical study of the breakdown field for over 100 top gated structures fabricated in different conditions and with different surface areas. Adopting a failure analysis based on the Weibull distribution, we show that the most reliable top gates are obtained when depositing in $\text{SiO}_2/\text{Ti}/\text{Au}$ without breaking the vacuum. Electron-beam SiO_2 layers evaporated in these ways have insulating characteristics as good as those of thermally grown SiO_2 layers.

5.1. Acknowledgments

S. Russo acknowledges financial support from Stichting voor Fundamenteel Onderzoek der Materie (FOM). M. F. Craciun acknowledges financial support from the Japan Society for the Promotion of Science, grant P07372. M. Yamamoto acknowledges Grant-in-Aid for Young Scientists A (no. 20684011) and Exploratory Research for Advanced Technology Japan Science and Technology Agency (08030000477). S. Tarucha acknowledges financial support from the Grant-in-Aid for Scientific Research S (no. 19104007), B (no. 18340081) and Japan Science and Technology Agency Core Research for Evolutional Science and Technology. A. F. Morpurgo acknowledges financial support from the Swiss National Science Foundation (grant 200021-121569) and from FOM.

- [1] Young A F and Kim P 2009 *Nature Phys.* 5 222
- [2] Meric I, Han M Y, Young A F, Ozyilmaz B, Kim P and Shepard K L 2008 *Nature Nanotech.* 3 654
- [3] Stander N, Huard B and Goldhaber-Gordon D 2009 *Phys. Rev. Lett.* 102 026807
- [4] Katsnelson M I, Novoselov K S and Geim A K 2006 *Nature Phys.* 2 620
- [5] Williams J R, Dirac L and Marcus C M 2007 *Science* 317 638
- [6] Huard B, Sulpizio J A, Stander N, Todd K, Yang B and Goldhaber-Gordon D 2007 *Phys. Rev. Lett.* 98 236803
- [7] Ozyilmaz B, Jarillo-Herrero P, Efetov D, Abanin D A, Levitov L S and Kim P 2007 *Phys. Rev. Lett.* 99 166804
- [8] Oostinga J B, Heersche H B, Liu X, Morpurgo A F and Vandersypen L M K 2008 *Nature Mater.* 7 151
- [9] Castro E V, Novoselov K S, Morozov S V, Peres N M R, Lopes dos Santos J M B, Nilsson J, Guinea F, Geim A K and Castro Neto A H 2007 *Phys. Rev. Lett.* 99 216802
- [10] Ohta T, Bostwick A, Seyller T, Horn K and Rotenberg E 2006 *Science* 313 951
- [11] McCann E 2006 *Phys. Rev. B* 74 161403
- [12] Craciun M F, Russo S, Yamamoto M, Oostinga J B, Morpurgo A F and Tarucha S 2009 *Nature Nanotech.* advanced online publication 26 April 2009, doi:10.1038/nnano.2009.89
- [13] Koshino M and McCann E 2009 *Phys. Rev. B* 79 125443
- [14] Blake P, Novoselov K S, Castro Neto A H, Jiang D, Yang R, Booth T J, Geim A K and Hill E W 2007 *Appl. Phys. Lett.* 91 063124
- [15] Todd K, Chou H T, Amasha S and Goldhaber-Gordon D 2009 *Nano Lett.* 9 (1) 416
- [16] Liu X, Oostinga J B, Morpurgo A F, Vandersypen L M K 2008 *arXiv:0812.4038*
- [17] Abergel D S L, Russell A and Falko V A 2007 *Appl. Phys. Lett.* 91 063125

- [18] Ni Z H, Wang H M, Kasim J, Fan H M, Yu T, Wu Y H, Feng Y P and Shen Z X 2007 Nano Letters 7 2758
- [19] These measurements on double gated devices were mainly carried out in a two terminal configuration. Measurements in a four terminal configuration confirmed that the influence of contact resistance present in two terminal devices did not influence significantly the results (see Supplementary online Information of Ref.[12] and Russo S, Craciun M F, Yamamoto M, Morpurgo A F M and Tarucha S 2009 arXiv:0901.0485)
- [20] Klein C A 1964 J. Appl. Phys. 35 2947
- [21] Novoselov K S, Geim A K, Morozov S V, Jiang D, Zhang Y, Dubonos S V, Grigorieva I V and Firsov A A 2004 Science 306 666
- [22] Wolters D R and Verwey J F 1986 Instabilities in Silicon Devices Amsterdam (Elsevier)
- [23] Lawless J F 1982 Statistical models and methods for lifetime data New York (John Wiley and Sons)
- [24] Sirea C, Blonkowski S, Gordon M J and Baron T 2007 Appl. Phys. Lett. 91 242905